

Article

Influence of Different Annealing Atmospheres on the Mechanical Properties of Freestanding MCrAlY Bond Coats Investigated by Micro-Tensile Creep Tests

Sven Giese ^{1,*}, Steffen Neumeier ¹ , Jan Bergholz ², Dmitry Naumenko ³,
Willem J. Quadakkers ³, Robert Vaßen ² and Mathias Göken ¹

¹ Materials Science & Engineering, Institute I, Friedrich-Alexander-Universität Erlangen-Nürnberg (FAU), Martensstr. 5, 91058 Erlangen, Germany; steffen.neumeier@fau.de (S.N.); mathias.goeken@fau.de (M.G.)

² IEK-1: Materials Synthesis and Processing, Institute of Energy and Climate Research, Forschungszentrum Jülich GmbH, Jülich 52425, Germany; Jan.Bergholz@de.rheinmetall.com (J.B.); r.vassen@fz-juelich.de (R.V.)

³ IEK-2, Institute of Energy and Climate Research, Forschungszentrum Jülich GmbH, Jülich 52425, Germany; d.naumenko@fz-juelich.de (D.N.); j.quadakkers@fz-juelich.de (W.J.Q.)

* Correspondence: sven.giese@fau.de; Tel.: +49-09131-85-27475

Received: 22 May 2019; Accepted: 17 June 2019; Published: 19 June 2019



Abstract: The mechanical properties of low-pressure plasma sprayed (LPPS) MCrAlY (M = Ni, Co) bond coats, Amdry 386, Amdry 9954 and oxide dispersion strengthened (ODS) Amdry 9954 (named Amdry 9954 + ODS) were investigated after annealing in three atmospheres: Ar–O₂, Ar–H₂O, and Ar–H₂–H₂O. Freestanding bond coats were investigated to avoid any influence from the substrate. Miniaturized cylindrical tensile specimens were produced by a special grinding process and then tested in a thermomechanical analyzer (TMA) within a temperature range of 900–950 °C. Grain size and phase fraction of all bond coats were investigated by EBSD before testing and no difference in microstructure was revealed due to annealing in various atmospheres. The influence of annealing in different atmospheres on the creep strength was not very pronounced for the Co-based bond coats Amdry 9954 and Amdry 9954 + ODS in the tested conditions. The ODS bond coats revealed significantly higher creep strength but a lower strain to failure than the ODS-free Amdry 9954. The Ni-based bond coat Amdry 386 showed higher creep strength than Amdry 9954 due to the higher fraction of the β-NiAl phase. Additionally, its creep properties at 900 °C were much more affected by annealing in different atmospheres. The bond coat Amdry 386 annealed in an Ar–H₂O atmosphere showed a significantly lower creep rate than the bond coat annealed in Ar–O₂ and Ar–H₂–H₂O atmospheres.

Keywords: MCrAlY; TMA; creep; bond coat; hydrogen; water vapor

1. Introduction

Many scientific studies have been carried out to investigate the oxidation behavior of MCrAlY bond coats and intermetallic coatings in varying environments. However, far fewer investigations have been performed for bond coats used in environments bearing hydrogen or water vapor. One strategy to reduce the CO₂ emissions of power plants is to use a H₂-enriched syngas in gas turbines [1]. By using syngas with hydrogen or water vapor instead of natural gas, some problems may arise. The negative effect of hydrogen embrittlement in iron and steels has been well-known for decades [2]. Some studies investigated the influence of water vapor and especially hydrogen on the formation and agglomeration of nanovoids and vacancies in various materials [3,4]. Vacancy clusters were found in Ni alloys by measuring the variation in positron lifetime and the intensity of hydrogen-charged samples. These investigations revealed that grain boundaries are the preferred regions in which hydrogen can facilitate

and stabilize vacancy clusters [3]. In addition, the diffusion of vacancies from the surface to the interior of the sample, which led to the formation of 20–200 nm holes, was observed in Ni samples after high temperature heat treatment [4]. The same behavior was found in Ni-base superalloys in which strain-induced agglomeration of vacancies during plastic deformation was observed by Takai et al., promoting fracture in Inconel 625 due to the creation of microvoids [5]. Furthermore, charging samples with hydrogen led to a remarkable reduction of the ductility of the Ni-base superalloy Inconel 718 during tensile tests by the coalescence of voids promoting crack initiation and propagation [6]. Localized deformation and stress concentration at grain boundaries and the growth and coalescence of voids led to the final failure of hydrogen-charged samples [7]. The formation of hydrogen bubbles and the agglomeration of voids was also observed, leading to blistering of the material and a general decrease of its mechanical properties [4,8]. Another problem caused by the addition of water vapor was the partially observed earlier spallation of thermal barrier coatings (TBCs) during cyclic tests [9].

The influence of H₂ and H₂O on the oxidation behavior of MCrAlY bond coats was investigated before by Zhou et al. as well as by Sullivan and Mumm [10,11]. The addition of water vapor led to an increase of (Ni,Co)(Al,Cr)₂O₄ spinel formation in bond coats, which influences the bond coat stability, the thermally grown oxide, and the TBC lifetime until spallation in syngas-fired turbines [11]. It was found that a higher P_{H₂O} led to stronger spinel growth for Amdry 386 at a higher P_{O₂}. The highest amount of spinel formation was observed at high P_{H₂O} and low P_{O₂}. Leyens et al. investigated the influence of environments containing water vapor and hydrogen on the oxidation resistance of Ni-based coatings and noticed that the addition of water vapor led to a 25% increase of the total mass gain after a heat treatment at 1100 °C for 28 h [12]. Subanovic et al. [8] found blistering of 2 mm thick freestanding MCrAlY bond coats exposed in a H₂/H₂O atmosphere. The effect was attributed to hydrogen release into the coating from the reaction between yttrium and water vapor and the subsequent formation of hydrogen gas at the internal coating defects (pores). Few experiments on freestanding bond coats have compared the influence of atmospheres containing H₂O and/or H₂ on creep properties. Micro-tensile creep testing of miniaturized samples under uniaxial loading has been used to evaluate the mechanical properties at the sub-micrometer scale [13–16]. A new testing methodology has recently been suggested in [17] where cylindrical samples were tested in a thermomechanical analyzer (TMA). The aim of this work is to investigate the effect of the heat treatment of freestanding Ni- and Co-bond coats under three different atmospheres containing oxygen, water vapor and hydrogen on creep resistance.

2. Experimental Methods

2.1. Material

Three MCrAlY bond coats were investigated in this work: A Ni-based bond coat, Amdry 386, and the two Co-based bond coats Amdry 9954, and oxide dispersion strengthened (ODS) Amdry 9954—the latter containing 2 wt.-% of Al₂O₃ for oxide dispersion strengthening. The chemical compositions are listed in Table 1.

Table 1. Atmospheres and nominal composition of Amdry 386 and oxide dispersion strengthened (ODS) Amdry 9954 in at.-% and O in ppm.

Material	Ni	Co	Al	Cr	Si	Y	Hf	O
Amdry 386	40.35	18.97	23.04	16.49	0.79	0.36	0.08	<500
Amdry 9954	28.68	34.18	15.57	21.25	0.13	0.32	-	<500
Amdry 9954 + ODS	28.82	34.01	17.14	20.14	0.05	0.20	-	9650

The coatings were produced by low-pressure plasma spraying (LPPS) on a steel substrate. To obtain freestanding bond coats, the steel substrate was spark eroded afterwards. A first homogenization annealing under an argon atmosphere for 2 h at 1100 °C was done. A second heat treatment was carried out for each bond coat in argon with additions of 20% O₂, 2% H₂O or 4% H₂ + 2% H₂O for 72 h at 1100 °C.

2.2. Sample Preparation

The exposed freestanding bond coat specimens were sliced with a precision wet abrasive cutting machine Brillant 220 (ATM GmbH, Mammelzen, Germany) from atm into a rectangular shape with a width of about 600 μm . For small-scale tensile testing, a circular sample cross section is recommended, resulting in a more reproducible manufacturing of the samples and equal testing conditions. These are huge advantages compared to the production of miniaturized samples with common fabrication methods like electrical discharge machining or mechanical milling [18,19]. To produce a cylindrical tensile specimen without notches and with high accuracy, the abrasive sliced samples were sent to Microsample GmbH in Austria for further preparation. The production of the miniaturized samples is described in detail in the work of Rathmayr et al. [20,21]. The cross sections of the samples were determined to be $450 \pm 2 \mu\text{m}$ in diameter over a gauge length of 2500 μm . Microstructural analysis was performed with a Zeiss Crossbeam 540 (Zeiss GmbH, Oberkochen, Germany) with backscattered electron images (BSE). The grain sizes and individual phase fractions of all the bond coats were determined by electron backscatter diffraction (EBSD) (Oxford Instruments, Abingdon, UK) with the software ATZEC from Oxford Instruments. Polished sections of the tested specimens after creep experiments along the testing direction were characterized by ImageJ (version 1.46r, Wayne Rasband, Bethesda, Rockville, MD, USA).

2.3. Experimental Setup

Micro-tensile creep tests were carried out with a thermomechanical analyzer (TMA) type 402 F3 Hyperion from Netzsch (Netzsch, Selb, Germany)—see also [17] for more details. The experimental setup consists of a SiC furnace with a constant flow of 400 mL/min of Ar during testing. The sample holder, the pushrod and the clamping jaws for mounting the samples are made of alumina, which is thermally stable up to 1550 $^{\circ}\text{C}$. The measuring system is thermally stabilized by constant water cooling during the experiments. Creep tests were performed at temperatures of 900–950 $^{\circ}\text{C}$. A constant load of 50 mN was applied for fixing the samples during heating with 5 K/min until the testing temperature was achieved. A holding period of 90 min was used for reaching thermal equilibrium before testing. The force of the load-controlled experiment was increased from 0.05 N to 2.37 N in 1 min, resulting in a stress of 15 MPa in the 450 μm diameter at the beginning of the experiments. The TMA setup and a micro tensile specimen before testing can be seen in Figure 1.

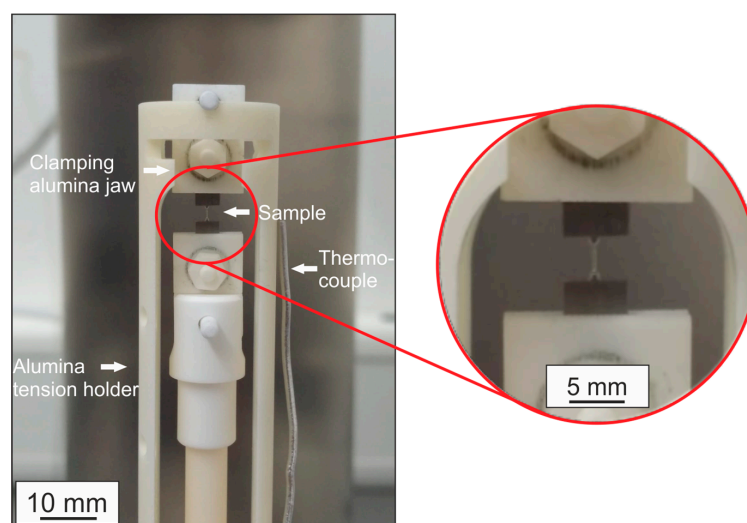


Figure 1. Thermomechanical analyzer (TMA) setup: alumina tension holder, pushrod and clamping jaw for mounting the sample. The polished tensile specimen has a diameter of 450 μm over the entire gauge length of 2500 μm before creep testing.

3. Results

3.1. Microstructure at the Initial State

The microstructures of Amdry 386, Amdry 9954 and Amdry 9954 + ODS after heat treatment at 1100 °C for 72 h in Ar–O₂, Ar–H₂O and Ar–H₂–H₂O are shown in Figure 2. No detrimental effect of oxygen, water vapor or hydrogen for all bond coats can be seen by microstructural analysis before the creep experiments. Blistering of the bond coats due to internal recombination of hydrogen, as described by Subanovic et al., was not found [8], probably due to a smaller Y-reservoir in the creep specimens associated with a smaller specimen thickness.

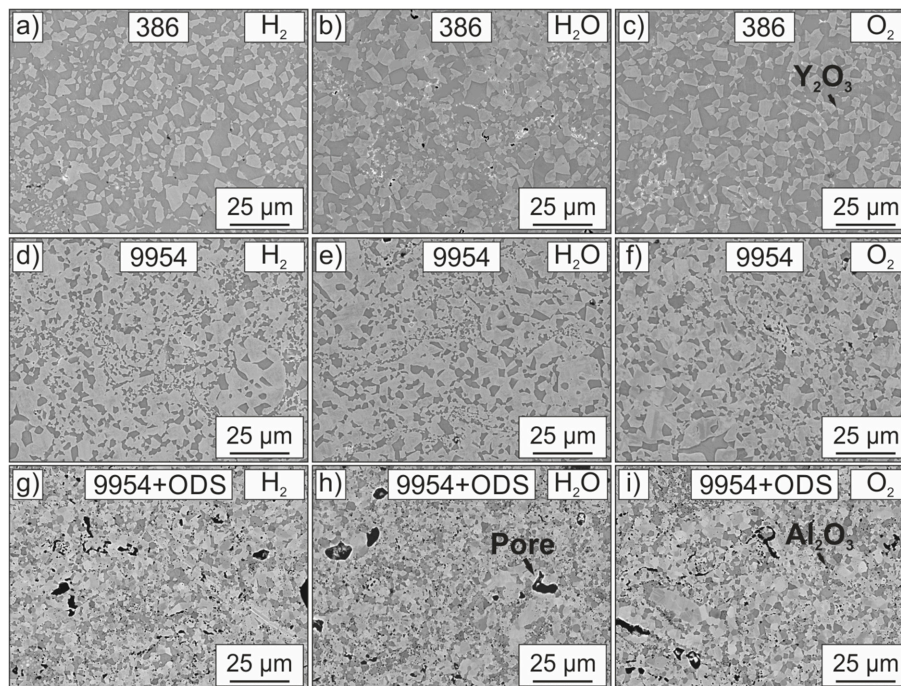


Figure 2. BSE (backscattered electron) images of the microstructures of Amdry 386 (a–c), Amdry 9954 (d–f) and Amdry 9954 + ODS (g–i) after a heat treatment of 72 h in Argon with the addition of 4% H₂ + 2% H₂O, 2% H₂O and 20% O₂ before creep testing.

Differences regarding the microstructure can only be attributed to the varying content of the β -NiAl phase and the γ -solid solution phase between Amdry 386 and Amdry 9954, as described in a previous study [17]. The formation of internal Y-rich oxides could be observed in all bond coats, similarly to the study by Huang et al. [22]. In addition to the two-phase β/γ -microstructure of Amdry 386 and Amdry 9954, the ODS-containing bond coats showed small, finely distributed alumina particles as well as accumulation of alumina.

Due to insufficient melting during the plasma spraying process, large, not completely molten particles were found in all specimens, especially in Amdry 9954 and 9954 + ODS. The inhomogeneous microstructure may have a negative effect on the mechanical properties of these alloys [23,24].

Due to the manufacturing process, a higher porosity of $2.1 \pm 0.48\%$ was found in the ODS-containing bond coats (Figure 2g–i) as opposed to $0.6 \pm 0.17\%$ in Amdry 386 and Amdry 9954. Figure 3 shows the grain size in all different conditions, analyzed by EBSD. As can be seen, the average grain size of 0.8–1.1 μm was not influenced by the varying atmospheres during the heat treatment. The ODS-containing bond coats revealed smaller areas of particles that were not completely molten and show a maximum grain size of 5–6 μm , significantly smaller than Amdry 386 and Amdry 9954. The sizes of all phases, as well as the phase fractions of each bond coat, were analyzed as well. Neither the

individual size of the β -NiAl phase, γ -solid solution and the alumina particles, nor the phase fraction was significantly influenced by heating in oxygen-, water vapor- or hydrogen-containing atmospheres.

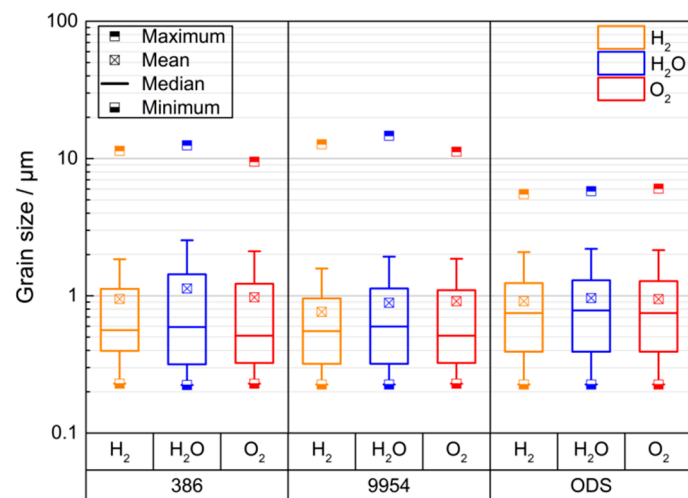


Figure 3. Distribution of the grain sizes of Amdry 386, Amdry 9954 and Amdry 9954 + ODS after a heat treatment at 1100 °C for 72 h in argon with the addition of 4% H₂ + 2% H₂O, 2% H₂O and 20% O₂.

3.2. Micro-Tensile Creep Experiments

The bond coats Amdry 386, Amdry 9954 and Amdry 9954 + ODS, which were heat treated in Ar–O₂, Ar–H₂O, and Ar–H₂–H₂O atmospheres at 1100 °C for 72 h were crept at testing temperatures of 900–950 °C. The results of the micro-tensile creep experiments are shown in Figure 4. Amdry 386 shows generally lower creep minima compared to Amdry 9954. Furthermore, it is obvious that the addition of 2 wt.-% of Al₂O₃ particles can significantly increase the creep resistance of MCrAlY bond coats.

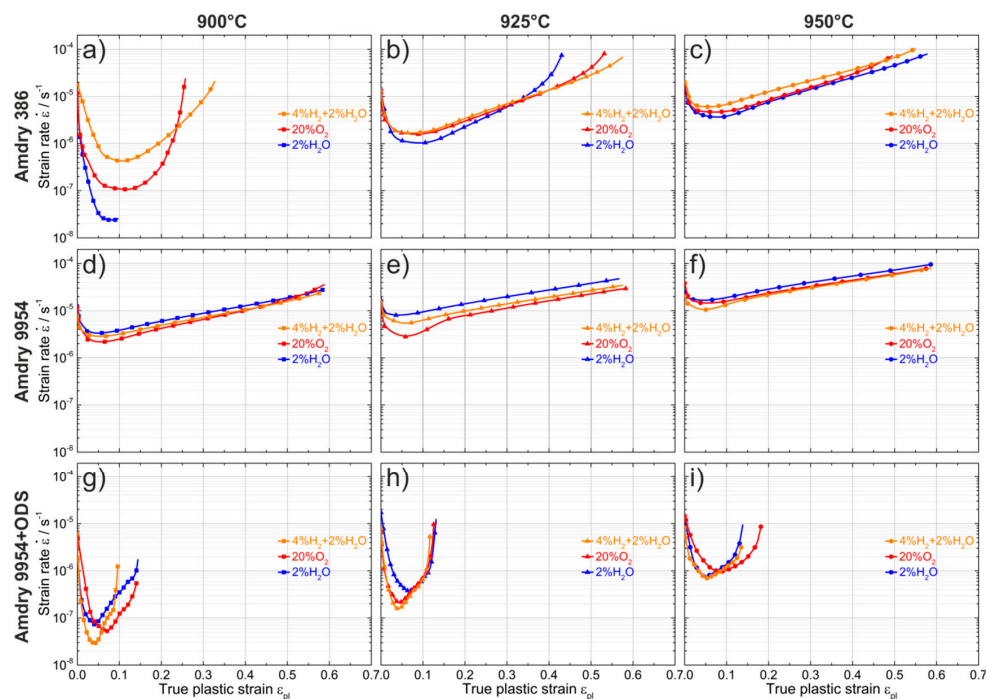


Figure 4. Strain rate versus true plastic strain plots at testing temperatures of 900–950 °C with an applied stress of 15 MPa. Before creep testing, Amdry 386 (a–c) Amdry 9954 (d–f) and Amdry 9954+ODS (g–i) were heat treated at 1100 °C for 72 h in Argon with the addition of 4% H₂ + 2% H₂O, 20% O₂ and 2% H₂O.

The most significant effect of heat treatment atmosphere on the creep behavior can be seen in Amdry 386 tested at 900 °C. The sample heat treated in Ar–H₂O showed the lowest creep minima, whereas the sample heat treated in Ar–H₂–H₂O showed a creep rate of more than one order of magnitude faster. The sample heat treated in Ar–H₂O was stopped after passing the creep minima at 627 h. With increasing temperature, the discrepancy diminished and the influence of the different atmospheres seemed to decline. The creep minima at all testing temperatures were reached at 0.06–0.1 plastic strain, though it was reached earlier at higher temperatures. Among the experiments with Amdry 386, the samples annealed in Ar–H₂O revealed lower creep minima than those annealed in Ar–H₂–H₂O and Ar–O₂, as indicated by the time to failure T_f in Table 2.

Table 2. Time to failure T_f for Amdry 386, Amdry 9954 and Amdry 9954 + ODS annealed in different atmosphere after creep experiments at 900–950 °C.

Material	Atmosphere	T_f /h 900 °C	T_f /h 925 °C	T_f /h 950 °C
Amdry 386	4% H ₂ + 2% H ₂ O	94	37	11
	2% H ₂ O	627	52	17
	20% O ₂	362	40	14
Amdry 9954	4% H ₂ + 2% H ₂ O	27	14	7
	2% H ₂ O	23	10	5
	20% O ₂	32	21	6
Amdry 9954 + ODS	4% H ₂ + 2% H ₂ O	438	102	34
	2% H ₂ O	235	53	29
	20% O ₂	355	84	31

For Amdry 9954, much higher creep rates than the Ni-based bond coat were observed in all experimental conditions. With increasing temperature, the creep rates of all samples annealed in different atmospheres increased slightly. Although the creep curves show almost the same progression, the samples heated in Ar–O₂ and Ar–H₂–H₂O had a tendency to have slightly lower creep minima than those heat treated in Ar–H₂O, at all temperatures. The high creep rate made it difficult to determine the possible influence of the individual atmospheres. Furthermore, the trend of the creep resistance of Amdry 9954 seemed to follow the opposite way to the sequence of Amdry 386. The highest creep rate and the longest time to failure could be related to the samples annealed in Ar–H₂O, whereas those annealed in Ar–H₂–H₂O and Ar–O₂ showed slightly lower creep rates. In the temperature range of 900–950 °C, all heat treatment variations showed the same creep curve progressions and strain to failure.

A remarkable decrease of the strain to failure from 0.6 without ODS particles to 0.1–0.2 with ODS particles was observed. The creep curves of Amdry 9954 + ODS were characterized by distinct creep minima, followed by a subsequent steep rise of the creep curves. The influence of oxygen, water vapor and hydrogen is difficult to interpret. However, the creep curves showed a similar tendency as in the oxide dispersion free alloy Amdry 9954. Samples annealed in Ar–H₂–H₂O and Ar–O₂ showed lower creep minima than those annealed in Ar–H₂O, especially at lower testing temperatures of about 900 °C and 925 °C. At 950 °C, the creep minima were virtually independent of the annealing atmosphere.

In Figure 5, the comparison of the creep minima for all nine experimental conditions and the corresponding activation energies are summarized.

Amdry 386 showed higher activation energies than Amdry 9954 due to the higher amount of β -NiAl. Associated with the lower creep minima of Amdry 386 annealed in Ar–H₂O, especially at 900 °C, it revealed the highest activation energy. The ODS particles significantly improved the creep resistance. However, the difference in activation energies is moderate due to the uniform changes of the creep minima with the increasing temperature.

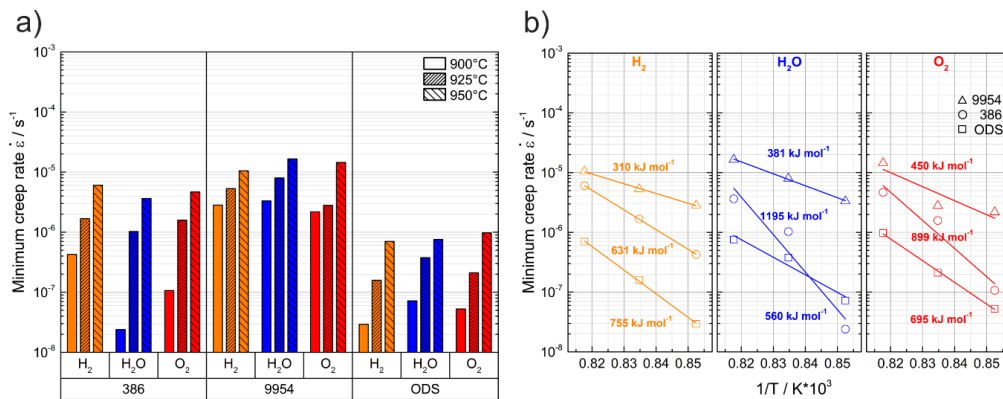


Figure 5. Minima creep rates (a) and activation energies (b) of testing temperatures of 900–950 °C. The samples of Amdry 386, Amdry 9954 and Amdry 9954 + ODS were heat treated before creep testing in Argon with the additions of 4% H_2 + 2% H_2O , 2% H_2O and 20% O_2 .

3.3. Microstructure after Creep Experiments

Figure 6 exemplifies an overview of all three bond coats tested in small-scale creep experiments at 900 °C with a stress of 15 MPa. The microstructures of the crept samples revealed significant differences between the three kinds of MCrAlY bond coats. These differences, which are due to the varying amounts of the high temperature stable β -NiAl phase and the oxide dispersion particles, were already investigated in a previous study [17]. The most substantial influence of the different atmospheres during annealing was observed in Amdry 386. The experiment of the sample annealed in Ar- H_2O was stopped after 627 h. Afterwards, it was cut at the thinnest position. No significant inner failure in the form of internal cracking could be noticed, as shown in Figure 6a. This was more pronounced in the Ar- H_2 - H_2O and Ar- O_2 samples since they were crept until failure, as shown in Figure 6b,c. It can be assumed that the cracks and pores were generated in the tertiary creep regime during tensile testing because almost no porosity was found in the regions of the grip sections of the Amdry 386 and Amdry 9954 specimens.

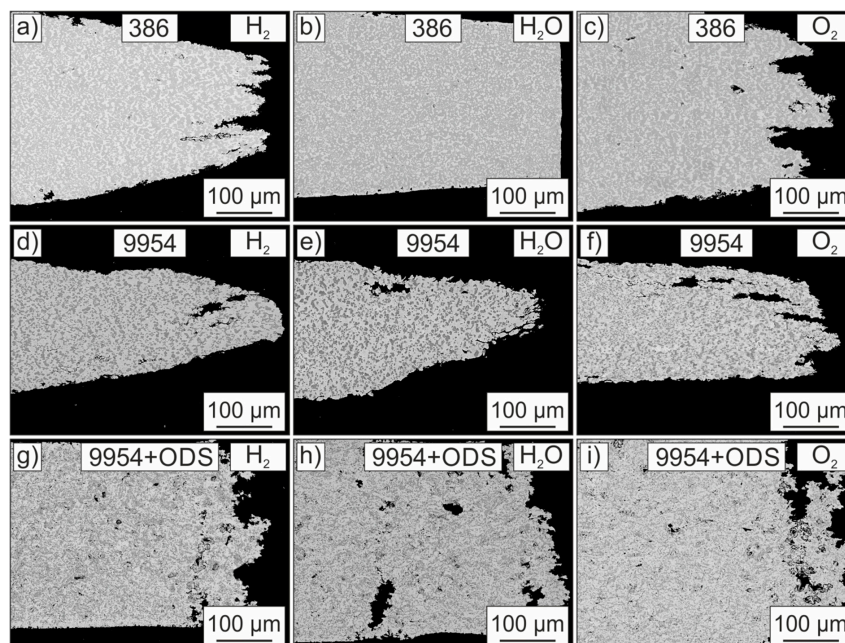


Figure 6. BSE images of the microstructures of Amdry 386 (a–c), Amdry 9954 (d–f) and Amdry 9954 + ODS (g–i) after tensile creep tests at 900 °C. Before creep testing, the samples were heat treated in Argon with the additions of 4% H_2 + 2% H_2O , 2% H_2O and 20% O_2 .

Based on the strong ODS effect of the Al_2O_3 particles, the ODS-containing bond coats failed much earlier than Amdry 9954, resulting in a more furrowed fracture surface.

4. Discussion

Amdry 386 showed superior creep properties compared to the Co-based bond coat Amdry 9954. The higher creep strength of β -NiAl, in contrast with the Ni- and Co-containing γ -solid solution phase, at temperatures above 900 °C, is responsible for the better creep resistance [24–26]. The higher yttrium content in Amdry 386 compared to Amdry 9954 led to the formation of smaller Y_2O_3 particles. These nanoscale oxide particles provide an additional hindering effect for deformation and therefore improve the mechanical properties. The beneficial influence of small oxide particles is also shown by the lower creep minima of the ODS-containing bond coat. Investigations by Arzt et al. of yttria-oxide particle-strengthened NiAl with a similar grain size as the bond coats investigated in this study showed that the additional hindering effect can be attributed to the interaction between dislocations and dispersoids in the material [27–29]. It is assumed that the nanoscale Al_2O_3 particles in Amdry 9954 + ODS have a similar dispersion strengthening effect and hinder the dislocation motion during creep testing. The better creep properties of Amdry 9954 + ODS come along with a lower ductility than Amdry 9954. In contrast, the observed differences in the creep behavior of the bond coats annealed in different atmospheres are more difficult to interpret. At low testing temperatures of 900 °C, significant differences were observed for Amdry 386, while testing at higher temperatures, as well as for the two Co-based bond coats, revealed only a slightly different creep behavior due to the annealing in different atmospheres. The reason for this difference will be discussed in the following section.

The influence of external oxidation during heat treatment at 1100 °C for 72 h in different atmospheres on the mechanical properties can be ignored in this study because the micro tensile samples were taken from the center of the bulk material. However, according to the literature, the addition of water vapor and hydrogen can promote internal oxidation [30]. Water vapor can lead to an increase of the oxygen vacancy concentration and an enhanced outward diffusion of aluminum [30–32]. Furthermore, water vapor extends the early initial stage of oxidation of Al-rich bond coats, hence stabilizing the transient θ -alumina stage [33]. Therefore, the less dense θ -alumina allows more oxygen to pass through the oxide layer, promoting the formation of external and internal α - Al_2O_3 [11,27]. Huang et al. showed that samples annealed in Ar– O_2 revealed an increased grain boundary diffusion for oxygen, resulting in a more pronounced internal oxidation than in Ar– H_2 – H_2O [22]. However, according to microstructural analysis, no internal oxidation could be observed in all bond coats and atmosphere compositions in the present study.

Further, neither the grain size, phase fraction, nor the phase size varied in the bond coats annealed in different atmospheres. The high creep rate of Amdry 386 annealed in Ar– H_2 – H_2O could be due to the interaction of hydrogen inside the bulk material with grain boundaries and interfaces. Investigations of tensile testing of Ni-based superalloys under hydrogen charging have revealed that hydrogen can enhance localized plasticity, which is known as the hydrogen-enhanced localized plasticity (HELP) mechanism. Fracture was mainly due to this localized plasticity and transgranular cracking was observed [7]. It was suggested that hydrogen promotes the coalescence and widening of voids during deformation, resulting in an easier crack propagation [6]. Takahashi et al. found that the hydrogen-enhanced decohesion (HEDE) mechanism, which was originally developed to explain the weakening of metallic bonds in bulk materials, can also be applied to small-scale specimens [34]. Therefore, the poorer creep behavior of the Amdry 386 sample annealed in Ar– H_2 – H_2O might be due to a combination of the interaction of hydrogen with grain boundaries and a decrease of the energy barrier for dislocation motion, which leads to an enhanced plasticity and earlier crack propagation.

5. Conclusions

One Ni-based and two Co-based freestanding bond coats with and without ODS particles annealed at 1100 °C for 72 h in argon atmospheres, containing additions of 20% O_2 , 2% H_2O and 4% H_2 + 2%

H₂O were investigated by micro-tensile creep tests. The force-controlled creep experiments were performed in a TMA at testing temperatures of 900–950 °C under constant Ar-flow and a constant load of 2.37 N. The higher amount of β-NiAl in the NiCoCrAlY—bond coat Amdry 386—led to superior creep properties than in the CoNiCrAlY—bond coat Amdry 9954. The addition of ODS particles to Amdry 9954 led to the highest creep resistance due to particle strengthening. For the Ni-based bond coat Amdry 386, the best creep properties were observed for samples annealed in Ar–H₂O. The influence of the atmospheres diminished at higher testing temperatures. For Amdry 9954, the influence of the different atmospheres was difficult to distinguish given the high creep rates at 900–950 °C with an applied stress of 15 MPa. However, both Co-based bond coats with and without ODS particles showed the lowest creep resistance after the addition of water vapor.

Author Contributions: Conceptualization, W.J.Q., R.V. and M.G.; methodology, M.G.; software, S.G.; validation, S.G. and S.N.; formal analysis, S.G.; investigation, S.G.; resources, J.B. and D.N.; data curation, S.G., S.N. and M.G.; writing—original draft preparation, S.G.; writing—review and editing, S.N. and M.G.; visualization, S.G.; supervision, S.N. and M.G.; project administration, S.N. and M.G.; funding acquisition, M.G.

Funding: This research was funded by the Deutsche Forschungsgemeinschaft (DFG) through projects A6 and B6 of the collaborative research centre SFB/TR 103 “From Atoms to Turbine Blades—a Scientific Approach for Developing the Next Generation of Single Crystal Superalloys”.

Acknowledgments: The authors are grateful to Ralf Laufs at IEK-1, Forschungszentrum Jülich GmbH, for supporting the production of samples. The authors would like to acknowledge Georg Rathmayr from Microsample GmbH for manufacturing the micro tensile specimen.

Conflicts of Interest: The authors declare no conflict of interest.

References

1. Chiesa, P.; Lozza, G.; Mazzocchi, L. Using Hydrogen as Gas Turbine Fuel. *J. Eng. Gas Turbines Power* **2005**, *127*, 73–80. [\[CrossRef\]](#)
2. Geng, W.T.; Wan, L.; Du, J.-P.; Ishii, A.; Ishikawa, N.; Kimizuka, H.; Ogata, S. Hydrogen bubble nucleation in α-iron. *Scr. Mater.* **2017**, *134*, 105–109. [\[CrossRef\]](#)
3. Lawrence, S.K.; Yagodzinsky, Y.; Hänninen, H.; Korhonen, E.; Tuomisto, F.; Harris, Z.D.; Somerday, B.P. Effects of grain size and deformation temperature on hydrogen-enhanced vacancy formation in Ni alloys. *Acta Mater.* **2017**, *128*, 218–226. [\[CrossRef\]](#)
4. Osono, H.; Kino, T.; Kurokawa, Y.; Fukai, Y. Agglomeration of hydrogen-induced vacancies in nickel. *J. Alloy. Compd.* **1995**, *231*, 41–45. [\[CrossRef\]](#)
5. Takai, K.; Shoda, H.; Suzuki, H.; Nagumo, M. Lattice defects dominating hydrogen-related failure of metals. *Acta Mater.* **2008**, *56*, 5158–5167. [\[CrossRef\]](#)
6. Zhang, Z.; Obasi, G.; Morana, R.; Preuss, M. Hydrogen assisted crack initiation and propagation in a nickel-based superalloy. *Acta Mater.* **2016**, *113*, 272–283. [\[CrossRef\]](#)
7. Tarzimoghadam, Z.; Ponge, D.; Klöwer, J.; Raabe, D. Hydrogen-assisted failure in Ni-based superalloy 718 studied under in situ hydrogen charging: The role of localized deformation in crack propagation. *Acta Mater.* **2017**, *128*, 365–374. [\[CrossRef\]](#)
8. Subanovic, M.; Naumenko, D.; Kamruddin, M.; Meier, G.; Singheiser, L.; Quadackers, W.J. Blistering of MCrAlY-coatings in H₂/H₂O-atmospheres. *Corros. Sci.* **2009**, *51*, 446–450. [\[CrossRef\]](#)
9. Déneux, V.; Cadoret, Y.; Hervier, S.; Monceau, D. Effect of Water Vapor on the Spallation of Thermal Barrier Coating Systems During Laboratory Cyclic Oxidation Testing. *Oxid. Met.* **2010**, *73*, 83–93. [\[CrossRef\]](#)
10. Zhou, C.; Yu, J.; Gong, S.; Xu, H. Influence of water vapor on the isothermal oxidation behavior of low pressure plasma sprayed NiCrAlY coating at high temperature. *Surf. Coat. Technol.* **2002**, *161*, 86–91. [\[CrossRef\]](#)
11. Sullivan, M.H.; Mumm, D.R. Transient stage oxidation of MCrAlY bond coat alloys in high temperature, high water vapor content environments. *Surf. Coat. Technol.* **2014**, *258*, 963–972. [\[CrossRef\]](#)
12. Leyens, C.; Fritscher, K.; Gehrling, R.; Peters, M.; Kaysser, W.A. Oxide scale formation on an MCrAlY coating in various H₂-H₂O atmospheres. *Surf. Coat. Technol.* **1996**, *82*, 133–144. [\[CrossRef\]](#)

13. Alam, Z.; Eastman, D.; Jo, M.; Hemker, K. Development of a High-Temperature Tensile Tester for Micromechanical Characterization of Materials Supporting Meso-Scale ICME Models. *JOM* **2016**, *68*, 2754–2760. [[CrossRef](#)]
14. Hemker, K.J.; Mendis, B.G.; Eberl, C. Characterizing the microstructure and mechanical behavior of a two-phase NiCoCrAlY bond coat for thermal barrier systems. *Mater. Sci. Eng. A* **2008**, *483–484*, 727–730. [[CrossRef](#)]
15. Hebsur, M.G.; Miner, R.V. Stress rupture and creep behavior of a low pressure plasma-sprayed NiCoCrAlY coating alloy in air and vacuum. *Thin Solid Films* **1987**, *147*, 143–152. [[CrossRef](#)]
16. Jaya, N.B.; Alam, M.Z. Small-scale mechanical testing of materials. *Curr. Sci.* **2013**, *105*, 1073–1099.
17. Giese, S.; Neumeier, S.; Amberger-Matschkal, D.; Bergholz, J.; Vaßen, R.; Göken, M. Micro-tensile creep testing of freestanding MCrAlY bond coats. *J. Mater. Res.* **2019**. [[CrossRef](#)]
18. Kumar, S.; Singh, R.; Singh, T.P.; Sethi, B.L. Surface modification by electrical discharge machining: A review. *J. Mater. Process. Technol.* **2009**, *209*, 3675–3687. [[CrossRef](#)]
19. Lee, L.C.; Lim, L.C.; Narayanan, V.; Venkatesh, V.C. Quantification of surface damage of tool steels after EDM. *Int. J. Mach. Tools Manuf.* **1988**, *28*, 359–372. [[CrossRef](#)]
20. Rathmayr, G.B.; Bachmaier, A.; Pippan, R. Development of a New Testing Procedure for Performing Tensile Tests on Specimens with Sub-Millimetre Dimensions. *J. Test. Eval.* **2013**, *41*, 20120175. [[CrossRef](#)]
21. Rathmayr, G.B.; Hohenwarter, A.; Pippan, R. Influence of grain shape and orientation on the mechanical properties of high pressure torsion deformed nickel. *Mater. Sci. Eng. A* **2013**, *560*, 224–231. [[CrossRef](#)] [[PubMed](#)]
22. Huang, T.; Bergholz, J.; Mauer, G.; Vassen, R.; Naumenko, D.; Quadackers, W.J. Effect of test atmosphere composition on high-temperature oxidation behaviour of CoNiCrAlY coatings produced from conventional and ODS powders. *Mater. High Temp.* **2018**, *35*, 97–107. [[CrossRef](#)]
23. Chen, H. Microstructure characterisation of un-melted particles in a plasma sprayed CoNiCrAlY coating. *Mater. Charact.* **2018**, *136*, 444–451. [[CrossRef](#)]
24. Chen, H.; Si, Y.Q.; McCartney, D.G. An analytical approach to the β -phase coarsening behaviour in a thermally sprayed CoNiCrAlY bond coat alloy. *J. Alloy. Compd.* **2017**, *704*, 359–365. [[CrossRef](#)]
25. Raj, S.V. Tensile creep of polycrystalline near-stoichiometric NiAl. *Mater. Sci. Eng. A* **2003**, *356*, 283–297. [[CrossRef](#)]
26. Karashima, S.; Oikawa, H.; Motomiya, T. Steady-state creep characteristics of polycrystalline nickel in the temperature range 500° to 1000 °C. *Trans. Jpn. Inst. Met.* **1969**, *10*, 205–209. [[CrossRef](#)]
27. Arzt, E.; Behr, R.; Göhring, E.; Grahle, P.; Mason, R.P. Dispersion strengthening of intermetallics. *Mater. Sci. Eng. A* **1997**, *234*, 22–29. [[CrossRef](#)]
28. Arzt, E.; Grahle, P. High temperature creep behavior of oxide dispersion strengthened NiAl intermetallics. *Acta Mater.* **1998**, *46*, 2717–2727. [[CrossRef](#)]
29. Grahle, P.; Arzt, E. Microstructural development in dispersion strengthened NiAl produced by mechanical alloying and secondary recrystallization. *Acta Mater.* **1997**, *45*, 201–211. [[CrossRef](#)]
30. Maris-Sida, M.C.; MEIER, G.H.; Pettit, F.S. Some Water Vapor Effects during the Oxidation of Alloys that are α -Al₂O₃ Formers. *Metall. Mater. Trans. A* **2008**, *34*, 2609–2619. [[CrossRef](#)]
31. Xing, L.; Zheng, Y.; Cui, L.; Sun, M.; Shao, M.; Lu, G. Influence of water vapor on the oxidation behavior of aluminized coatings under low oxygen partial pressure. *Corros. Sci.* **2011**, *53*, 3978–3982. [[CrossRef](#)]
32. Kaplin, C.; Brochu, M. Effects of water vapor on high temperature oxidation of cryomilled NiCoCrAlY coatings in air and low-SO₂ environments. *Surf. Coat. Technol.* **2011**, *205*, 4221–4227. [[CrossRef](#)]
33. Saunders, S.R.J.; Monteiro, M.; Rizzo, F. The oxidation behaviour of metals and alloys at high temperatures in atmospheres containing water vapour: A review. *Prog. Mater. Sci.* **2008**, *53*, 775–837. [[CrossRef](#)]
34. Takahashi, Y.; Kondo, H.; Asano, R.; Arai, S.; Higuchi, K.; Yamamoto, Y.; Muto, S.; Tanaka, N. Direct evaluation of grain boundary hydrogen embrittlement: A micro-mechanical approach. *Mater. Sci. Eng. A* **2016**, *661*, 211–216. [[CrossRef](#)]

